

# Structure-Guided Engineering of D-Carbamoylase Reveals a Key Loop at Substrate Entrance Tunnel

Yafei Liu,<sup>#</sup> Guochao Xu,<sup>#</sup> Jieyu Zhou, Jie Ni, Lu Zhang, Xiaodong Hou, Dejing Yin, Yijian Rao,<sup>\*</sup> Yi-Lei Zhao,<sup>\*</sup> and Ye Ni<sup>\*</sup>



Cite This: *ACS Catal.* 2020, 10, 12393–12402



Read Online

ACCESS |



Metrics & More



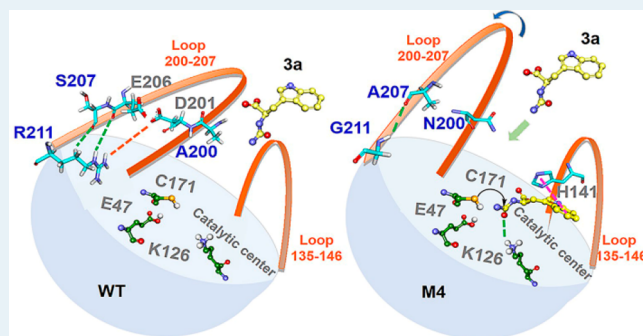
Article Recommendations



Supporting Information

**ABSTRACT:** A D-carbamoylase NiHyuC from *Nitratireductor indicus* was identified with high catalytic activity toward N-carbamoyl-D-tryptophan (3a). To further enhance its efficiency, both random mutagenesis and structure-guided evolution were performed. Variant M4 (D187N/A200N/S207A/R211G) showed a 43-fold increase in catalytic efficiency ( $k_{\text{cat}}/K_m = 1135.0 \text{ min}^{-1} \text{ mM}^{-1}$ ) and a 21-fold reduction in  $K_m$  value (0.4 mM) compared with WT. Crystal structures of beneficial variants were resolved to clarify the evolutionary changes underlying improvements to catalytic efficiency. Structure alignment with WT indicated that loop 200–207 may play an important role in modulating access to the substrate entrance tunnel. Furthermore, MD simulations of WT–3a and M4–3a interactions illustrated that M4–3a has a better angle for nucleophilic attack and more readily enters a prereaction state. Additional hydrogen bonds and hydrophobic interactions were observed in prereaction states of M4–3a compared with that of WT–3a, consistent with its decreased  $K_m$  value. In a hydantoinase process, the complete conversion of 160 mM L-indolylmethylhydantoin was achieved by M4 in a 0.5 L reaction, with D-tryptophan yield of 99.3% and productivity of  $64.9 \text{ g L}^{-1} \text{ d}^{-1}$ . This study reveals a key loop at the substrate tunnel of D-carbamoylase and provides an effective strategy for engineering D-carbamoylase and other carbon–nitrogen hydrolase family enzymes.

**KEYWORDS:** D-carbamoylase, structure-guided engineering, loop flexibility, catalytic efficiency, hydantoinase process, D-tryptophan



## INTRODUCTION

D-Amino acids are widely used in pharmaceutical and food industries. For example, D-alanine is used in the synthetic sweetener Alitame (with 2000-fold higher sweetness than sucrose);<sup>1</sup> D-phenylglycine is used in the synthesis of  $\beta$ -lactam antibiotics,<sup>2</sup> and D-tryptophan (D-Trp) is used in the synthesis of medications for the treatment of acromegaly (Octreotide) and for erectile dysfunction or benign prostatic hyperplasia (Tadalafil).<sup>3</sup> In 2016, Tadalafil alone accounted for over \$3 billion global sales. D-Trp can also be used to synthesize peptide drugs for dermatitis, including Tyrocidine C, Tyrocidine D, and Thymodepressin.<sup>3</sup> The Global Industry Analysis Corporation predicted that the global D-amino acid market is expected to reach over US \$171.1 million by 2025.<sup>4</sup> Therefore, the development of efficient and sustainable methods for D-amino acids synthesis is currently an area of great interest among researchers and drug developers.

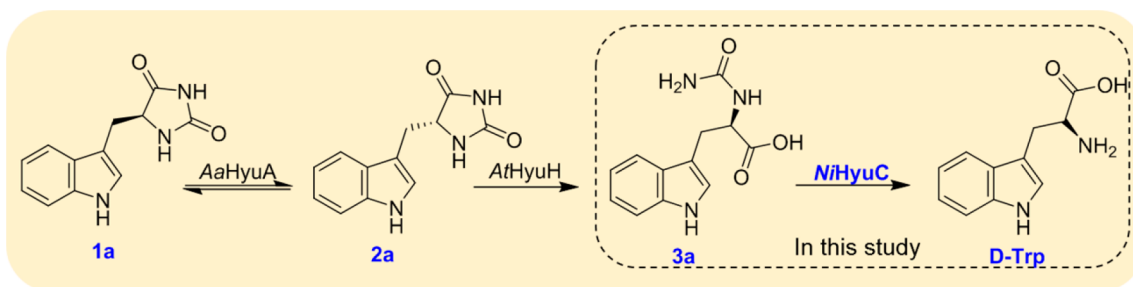
Biocatalytic approaches have a number of advantages over traditional chemical synthesis techniques, such as high stereoselectivity and benign reaction conditions. Moreover, biocatalytic approaches have been developed for synthesis of several D-amino acids that involve enzymes such as acylase,<sup>5</sup> lyase,<sup>6,7</sup> transaminase,<sup>8</sup> and the hydantoinase process. How-

ever, only a few enzymes can be used to synthesize D-amino acids that have large steric hindrances, such as D-Trp. In these cases, amidases<sup>9</sup> and aminoacylase<sup>10</sup> are primarily used to catalyze the resolution of racemic substrates to obtain D-amino acids and for which the theoretical yield is only 50%. The hydantoinase process (Scheme 1) is a three-enzyme cascade reaction that includes hydantoin racemase, hydantoinase, and carbamoylase. First, hydantoin racemase can racemize L- or D-hydantoin to obtain racemic hydantoin; the stereoselective hydantoinase catalyzes the hydrolysis of one hydantoin isomer to give the corresponding N-carbamoyl amino acid; the N-carbamoyl amino acid is then hydrolyzed by stereoselective carbamoylase, resulting in a chiral amino acid. Dynamic kinetic resolution of racemic hydantoins can be achieved, leading to a complete conversion of substrates.<sup>11–15</sup> The hydantoinase

Received: July 6, 2020

Revised: September 28, 2020

Published: September 28, 2020

Scheme 1. Hydantoinase Process for Producing D-Trp<sup>a</sup>

<sup>a</sup>1a: L-indolylmethylhydantoin; 2a: D-indolylmethylhydantoin; 3a: N-carbamoyl-D-tryptophan.

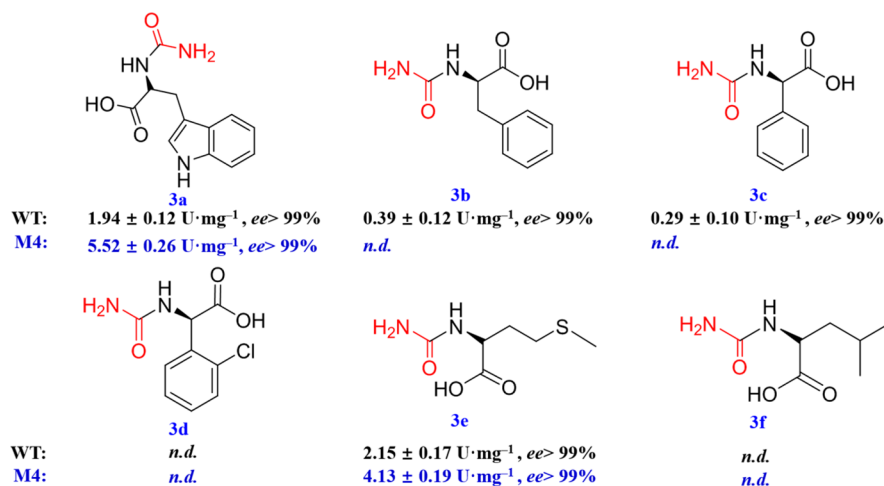


**Figure 1.** Substrate spectrum of NiHyuC WT and M4. All measurements were performed in triplicate at 2 mM substrate concentration. n.d. denotes no activity was detected.

process is an economical and environmentally friendly method for producing optically pure amino acids.

However, compared with hydantoin racemase and D-hydantoinase, D-carbamoylase has lower enzymatic activity and thermostability, which can limit its industrial application in synthesis of various amino acids.<sup>16–20</sup> Nozaki et al. reported a hydantoinase process for preparing 25 g L<sup>-1</sup> (109 mM) of D-Trp, in which 48 h was required to achieve 96% yield, due to the accumulation of intermediates.<sup>21</sup> In the preparation of D-Met, 6 h was required for the complete conversion of 2.61 g L<sup>-1</sup> substrate.<sup>22</sup> Protein engineering has been demonstrated to be a powerful approach for obtaining highly efficient biocatalysts, such as dehydrogenase,<sup>23–26</sup> transaminase,<sup>27</sup> monooxygenase,<sup>28,29</sup> lipase,<sup>30,31</sup> etc. In previous reports, protein engineering of D-carbamoylases has been mainly focused on enhancing thermostability or oxidative resistance. Ikenaka and co-workers obtained a series of D-carbamoylase variants from *Agrobacterium tumefaciens* with an improved thermostability of about 5–10 °C.<sup>32</sup> A mutant of D-carbamoylase originating from *Agrobacterium radiobacter* was obtained with enhanced resistance to oxidation but with 50% decreased enzymatic activity compared with wild-type (WT).<sup>33</sup> However, engineering D-carbamoylase for enhanced catalytic efficiency remains challenging, with a dearth of research in this area.

In this work, a D-carbamoylase NiHyuC was identified from *Nitratireductor indicus* CGMCC 1.10953. NiHyuC exhibited a higher activity (1.94 U mg<sup>-1</sup>) toward 3a and better thermostability ( $t_{1/2}$  of 72 h at 30 °C) than D-carbamoylase

from *Arthrobacter crystallopoietes* (AcHyuC).<sup>34</sup> To further improve the catalytic efficiency of NiHyuC, both random mutagenesis and structure-guided engineering were performed. Variant M4 (D187N/A200N/S207A/R211G) was obtained, which exhibited 43-fold higher catalytic efficiency than WT. To elucidate the structural changes that lead to the improvement of catalytic efficiency, crystallization and MD simulations were performed, in which a key loop at the substrate entrance tunnel of D-carbamoylase was identified. When applied in a cascade reaction, M4 was able to catalyze the complete conversion of 160 mM 1a for production of D-Trp.

## RESULTS AND DISCUSSION

**Identification of NiHyuC.** Here, using gene database mining, we identified a D-carbamoylase from *Nitratireductor indicus* CGMCC 1.10953, NiHyuC (Genebank accession number: EKF40735). It belongs to carbon–nitrogen hydrolase family and shares the highest sequence identity of 54.0% with a D-carbamoylase (PDB: 1FO6) from *Agrobacterium radiobacter*.<sup>33</sup> NiHyuC showed a soluble expression (Figure S1) and a desirable specific activity of 1.94 U mg<sup>-1</sup> toward 3a. In substrate spectrum analysis (Figure 1), NiHyuC exhibited catalytic activity toward N-carbamoyl-D-amino acids with relatively large steric hindrances, such as N-carbamoyl-D-phenylalanine (3b), N-carbamoyl-D-phenylglycine (3c), and N-carbamoyl-D-methionine (3e). Enantioselectivity analysis of NiHyuC showed that only D-enantiomer was catalyzed (Figure S2). The optimal reaction pH and temperature were pH 8.0 in Tris-HCl and 35 °C (Figure S3A,B), and its half-life was 72 h

**Table 1. Kinetic Parameters of NiHyuC and Its Variants Toward 3a and Their Yields in Cascade Reactions<sup>a</sup>**

variants	mutagenesis site	library	$K_m$ (mM)	$k_{cat}$ ( $\text{min}^{-1}$ )	$k_{cat}/K_m$ ( $\text{min}^{-1} \text{mM}^{-1}$ )	yield %
WT	none	/	$8.9 \pm 0.3$	$209.9 \pm 22.2$	$25.7 \pm 8.3$	$79.3^b$ $40.1^c$
D187N	D187N	epPCR	$1.1 \pm 0.2$	$134.8 \pm 5.9$	$121.4 \pm 11.1$	$94.9^b$
R211G	R211G	epPCR	$4.1 \pm 0.6$	$352.4 \pm 10.0$	$87.0 \pm 11.0$	$97.7^b$ $55.8^c$
A200E	A200E	SM	$1.9 \pm 0.3$	$177.8 \pm 9.0$	$96.4 \pm 11.9$	$97.8^b$
A200S	A200S	SM	$1.7 \pm 0.1$	$181.9 \pm 5.2$	$109.2 \pm 5.4$	$94.2^b$
A200N	A200N	SM	$2.2 \pm 0.3$	$190.9 \pm 15.3$	$88.6 \pm 12.3$	$92.7^b$
A200H	A200H	SM	$3.2 \pm 0.7$	$211.4 \pm 19.4$	$67.7 \pm 9.4$	$85.6^b$
E138Q	E138Q	SM	$24.2 \pm 4.7$	$1662.8 \pm 204.8$	$68.7 \pm 5.1$	$74.2^b$
E138W	E138W	SM	$4.5 \pm 0.3$	$506.0 \pm 13.8$	$112.6 \pm 4.4$	$93.8^b$
S207A	S207A	SM	$3.9 \pm 0.6$	$241.9 \pm 15.9$	$62.3 \pm 5.4$	$92.4^b$
M2-1	D187N/R211G	CM	$2.9 \pm 0.6$	$554.6 \pm 58.9$	$192.7 \pm 13.1$	$92.4^b$
M2-2	E138W/R211G	ICM	$1.5 \pm 0.4$	$415.9 \pm 41.5$	$286.1 \pm 50.3$	$63.8^c$
M2-3	S207A/R211G	ICM	$0.7 \pm 0.1$	$190.6 \pm 7.0$	$275.1 \pm 58.6$	$66.4^c$
M2-4	A200N/R211G	ICM	$1.7 \pm 0.2$	$415.9 \pm 17.3$	$246.1 \pm 18.9$	$65.0^c$
M3-1	D187N/A200N/R211G	ICM	$0.6 \pm 0.1$	$485.2 \pm 41.6$	$807.5 \pm 92.4$	$76.3^c$
M3-2	D187N/S207A/R211G	ICM	$0.8 \pm 0.1$	$481.8 \pm 27.7$	$638.1 \pm 47.9$	/
M3-3	A200N/S207A/R211G	ICM	$0.7 \pm 0.1$	$443.6 \pm 17.3$	$630.9 \pm 65.1$	/
M3-4	E138W/S207A/R211G	ICM	$1.0 \pm 0.2$	$594.1 \pm 48.5$	$600.2 \pm 54.3$	/
M4	D187N/A200N/S207A/R211G	ICM	$0.4 \pm 0.0$	$429.1 \pm 13.9$	$1135.0 \pm 83.5$	$79.1^c$

<sup>a</sup>A 10 mL reaction system containing 0.229 or 0.458 g **1a** (100 mM or 200 mM), 10 U mL<sup>-1</sup> AaHyuA, 10 U mL<sup>-1</sup> AtHyuH, 60 U mL<sup>-1</sup> NiHyuC WT or variants, and 0.25 mM MnCl<sub>2</sub> was carried out at 30 °C and 180 rpm. The reaction time was 24 h. <sup>b</sup>Yield was calculated with 100 mM **1a**. <sup>c</sup>Yield was calculated with 200 mM **1a**. epPCR: error prone PCR; SM: saturation mutagenesis; CM: combinatorial mutagenesis; and ICM: iterative combinatorial mutagenesis.

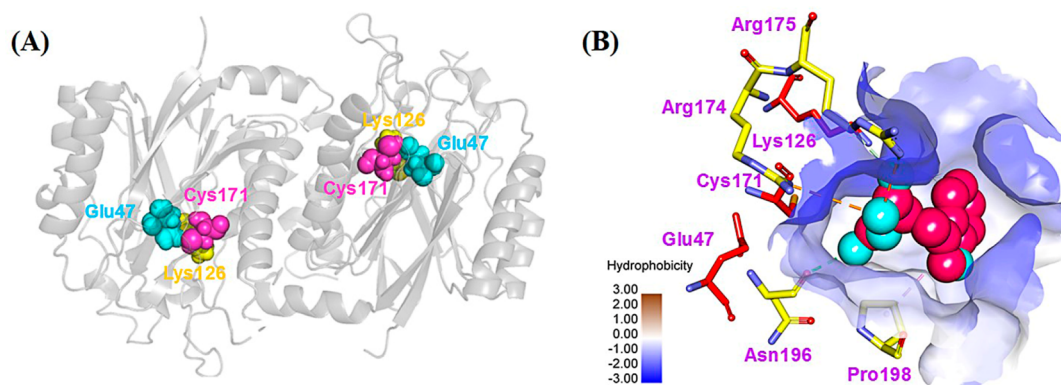


**Figure 2.** (A) Overall crystal structure of WT NiHyuC. Catalytic triads are shown as spheres. (B) Substrate binding pocket of NiHyuC. Catalytic triads are shown in red sticks, **3a** in CPK. CPK: Displays sphere sizes relative to van der Waals radii.

at 30 °C, representing 6-fold of AcHyuC (12 h) (Figure S3C, Table S1). Metal ions including Cu<sup>2+</sup>, Ni<sup>2+</sup>, and Zn<sup>2+</sup> severely inhibited its activity (Figure S3D). NiHyuC has a significantly higher  $k_{cat}$  value toward **3a** (209.9 min<sup>-1</sup>) compared with AcHyuC (39.5 min<sup>-1</sup>). Whereas its higher  $K_m$  value of 8.9 mM results in a moderate  $k_{cat}/K_m$  of 25.7 min<sup>-1</sup> mM<sup>-1</sup>, similar to that of AcHyuC (30.4 min<sup>-1</sup> mM<sup>-1</sup>) (Table S1).

After optimization, when coupling NiHyuC (60 U mL<sup>-1</sup>) with hydantoin racemase AaHyuA<sup>34</sup> (10 U mL<sup>-1</sup>) and D-hydantoinase AtHyuH<sup>34</sup> (10 U mL<sup>-1</sup>), a 79.3% yield resulted from 100 mM **1a** at 24 h. The intermediate *N*-carbamoyl-D-tryptophan (**3a**) was found to accumulate in this reaction, presumably due to unbalanced catalytic efficiency of AaHyuA ( $k_{cat}/K_m = 121.1 \text{ min}^{-1} \text{ mM}^{-1}$ ), AtHyuH ( $k_{cat}/K_m = 181.6 \text{ min}^{-1} \text{ mM}^{-1}$ ), and NiHyuC ( $k_{cat}/K_m = 25.7 \text{ min}^{-1} \text{ mM}^{-1}$ ). To examine this possibility, the cascade reaction was supplied with a 10-fold NiHyuC loading. This modification led to the

complete conversion of the substrate (Figure S4). These results indicated that the low catalytic efficiency of NiHyuC was mainly responsible for the relatively low product yield. Therefore, NiHyuC was subjected to further protein engineering for reduced  $K_m$  and enhanced catalytic efficiency.

**Random Mutagenesis.** A phenol red-based high-throughput screening method (Figure S5) was constructed and used to screen a library of 15,000 NiHyuC variants generated by error-prone PCR. Variants 1E8 (R211G) and 3D12 (D187N) exhibited significantly higher activity than that of WT. As shown in Table 1, R211G exhibited 50% reduced  $K_m$  (4.1 mM) and 0.68-fold enhanced  $k_{cat}$  (352.4 min<sup>-1</sup>). The  $k_{cat}/K_m$  of R211G was 87.0 min<sup>-1</sup> mM<sup>-1</sup>, 2.40-fold higher than that of WT (25.7 min<sup>-1</sup> mM<sup>-1</sup>). To evaluate its catalytic efficacy, a cascade reaction was performed that coupled the R211G variant with AaHyuA and AtHyuH at 100 mM **1a** substrate. This reaction provided a 100% substrate conversion and a D-

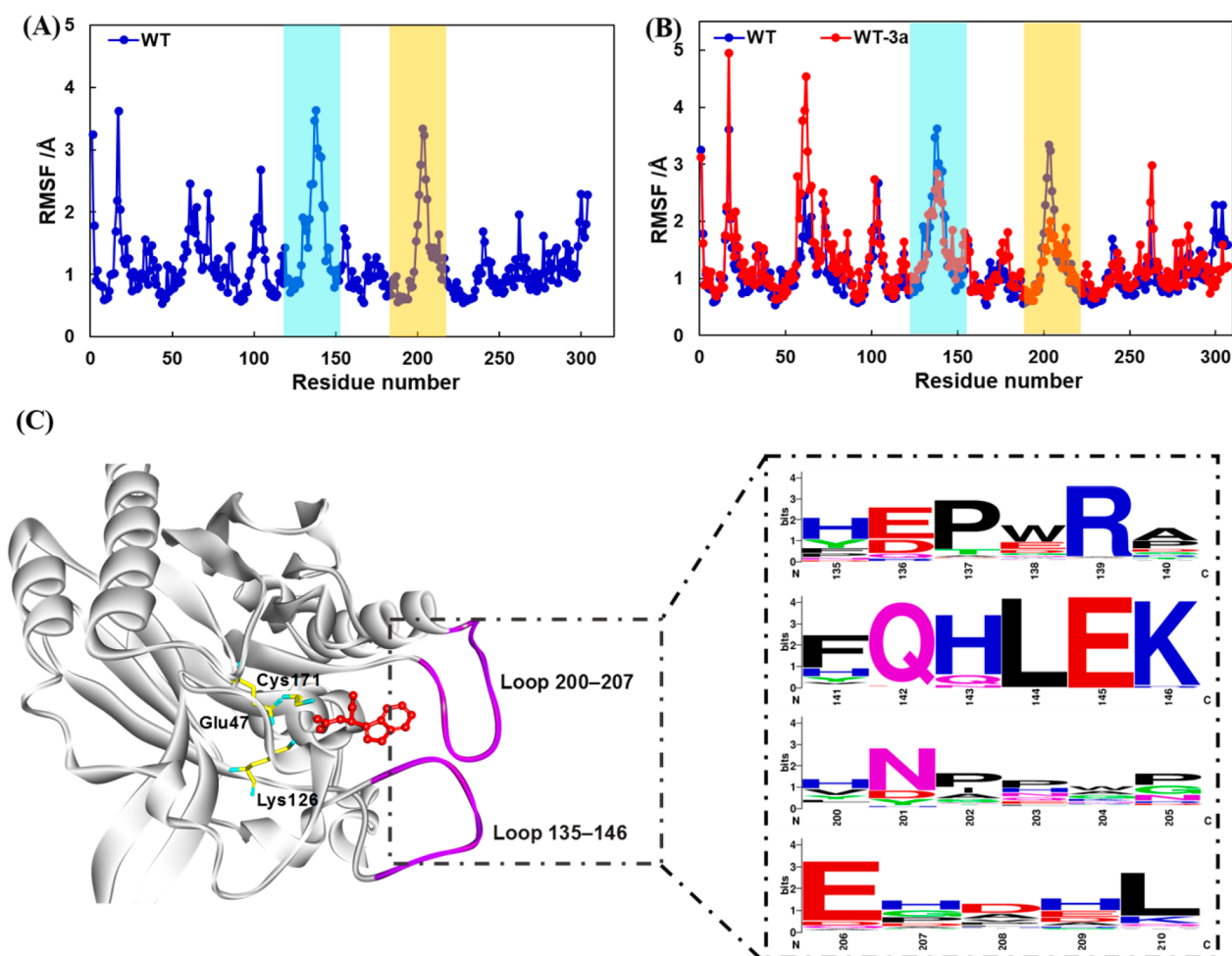


**Figure 3.** RMSF values for (A) *NiHyuC* WT and the (B) WT–3a complex. Substrate 3a was docked into WT with Discovery studio 4.5. The RMSF of atomic positions is calculated according to a reference frame in the trajectory, and the RMSF of residue is calculated by averaging the RMSF of atoms of each residue. The definition formula for RMSF is shown in Supporting Information. (C) Sequence conservation analysis of loops 135–146 and 200–207 based on 1000 various *D*-carbamoylases. The residue frequencies were constructed with WebLogo. Catalytic triads are shown as yellow sticks. Substrate 3a is shown as a red ball and stick model; purple indicates loops.

Trp yield of 97.7% at 24 h. Variant D187N had a dramatically reduced  $K_m$  of 1.1 mM, and a slightly decreased  $k_{cat}$  of 134.8  $\text{min}^{-1}$  compared with WT, and when coupled with *AaHyuA* and *AtHyuH*, the *D*-Trp yield was 94.9% after 24 h. Saturation mutagenesis of R211 and D187 did not result in more efficient variants than R211G and D187N (Figure S6). The D187N/R211G (M2–1) double mutant showed a further improved  $k_{cat}/K_m$  value of 192.7  $\text{min}^{-1} \text{mM}^{-1}$ , but the cascade reaction yielded 92.4% *D*-Trp, lower than the single mutants. Although the reaction started fast, it slowed down after 2 h and ended in a lower yield, which was potentially related to its low stability of M2–1 in the reaction system (data not shown). This result showed that the combination of D187N and R211G did not exhibit a synergistic effect. To further improve the catalytic efficiency and obtain mutants with high reaction performance, structure-guided engineering was performed.

**Identification of Core Residues through Evolutionary and MD Analysis.** In order to provide structural guidance for further protein engineering, the crystal structure of *NiHyuC* (PDB: 6LE1) was resolved at 2.80 Å (Table S4). The electron densities of main carbon chain and side chain are clear at this resolution except residues 204 and 205 (Figure S7A and Figure

S8A). *NiHyuC* is a homodimer and has a Glu47–Lys126–Cys171 catalytic triad (Figure 2A) and a strongly hydrophilic substrate binding pocket. To better understand the residues necessary for binding and catalysis, substrate 3a was docked into *NiHyuC* using Discovery studio 4.5 (Figure 2B). Interaction analysis indicates that the indole ring of 3a has a relatively weaker interaction with the hydrophilic substrate binding pocket, which may underlie the compromised affinity of *NiHyuC* toward 3a (Figure S9).

To improve the affinity of *NiHyuC* for 3a, 100 ns molecular dynamic (MD) simulations were performed on WT and WT–3a complexes. By extracting the root-mean-square fluctuation (RMSF) values of residue trajectories, significant fluctuations were observed in loops 135–146 and 200–207 (Figure 3A,B). For WT–3a complexes (Figure 3B), the RMSF values of both loops were lower than that of WT (Figure 3A), indicating these two loops may be closely involved in substrate binding.

Since flexible loop regions often participate in catalytic reactions,<sup>35</sup> it is possible that these loops may affect the substrate affinity of *NiHyuC*. Sequence conservation analysis of the evolution of these two loop regions revealed that the loop regions of 135–140 and 200–207 are nonconserved

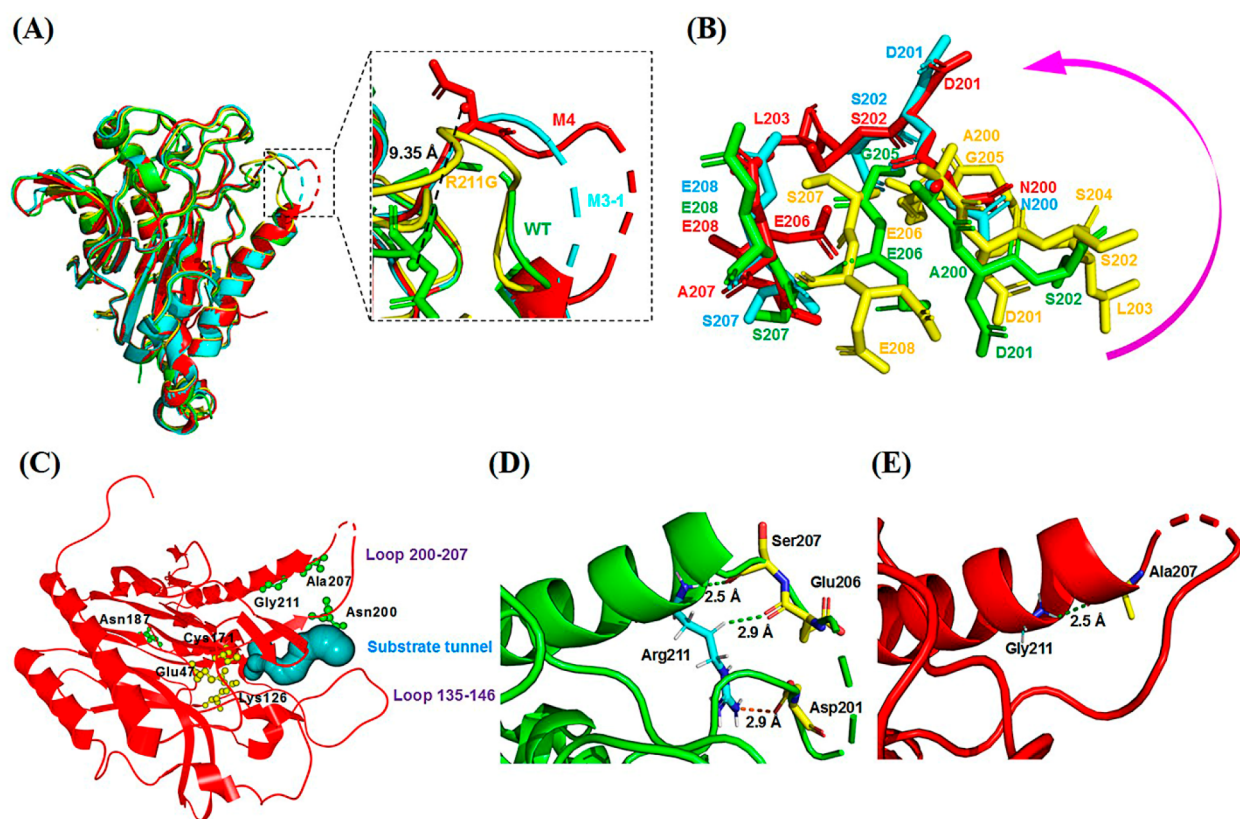


**Figure 4.** (A) Structure alignments of NiHyc WT and variants. WT, green; R211G, yellow; M3-1, cyan; and M4, red. The structures are displayed in cartoon by PyMOL. Since the electron density of residues 203 and 204 in WT, 203–206 in M3-1, 204, and 205 in M4 are missing, they are displayed as a dashed line. (B) Display of loop 200–207 in sticks. WT, green; R211G, yellow; M3-1, cyan; and M4, red. (C) Illustration of M4 mutation sites and substrate tunnel. Catalytic triads are shown in yellow ball and stick models; mutation sites are shown in green ball and stick models. Substrate tunnel is shown in cyan spheres, computed by CAVER analyst 2.0. Interaction analysis of (D) R211 and (E) G211 sites. Residues are shown as stick models. Hydrogen bonds are indicated by green dashed lines; attractive electrostatic interactions are indicated by an orange dashed line.

(Figure 3C), which may provide low evolutionary selective pressure. On the basis of these MD and sequence conservation analyses, ten residues were selected for further NNK codon-saturation mutagenesis, including Y135, E136, E138, S140, A200, S202, L203, S204, G205, and S207 (Figure S10). Seven positive variants, A200E, A200S, A200N, A200H, E138Q, E138W, and S207A were obtained (Table 1). Except for E138Q, all variants showed significantly reduced  $K_m$  values. When A200 was mutated to polar amino acids such as Glu, Ser, Asn, and His,  $K_m$  values decreased from 8.9 mM to 1.7–3.2 mM, although little effect was observed on the  $k_{cat}$  value. As a result, enhanced catalytic efficiencies ( $k_{cat}/K_m$ ) of 96.4, 109.2, 88.6, and 67.7  $\text{min}^{-1} \text{mM}^{-1}$  were achieved by the A200E, A200S, A200N, and A200H variants, respectively, representing 1.63–3.24 times higher catalytic efficiency than that of WT. When S207 was mutated to alanine, the result was a 50% reduced  $K_m$  value (3.9 mM) and 1.42-fold greater catalytic efficiency (62.3  $\text{min}^{-1} \text{mM}^{-1}$ ) compared with WT. For E138, two variants exhibited opposite effects on the  $K_m$  value. Specifically, E138W had an improved  $k_{cat}$  (506.0  $\text{min}^{-1}$ , 2.42-fold that of WT), a reduced  $K_m$  value (4.5 mM, half that of WT), and a catalytic efficiency of 112.6  $\text{min}^{-1} \text{mM}^{-1}$  (3.40-fold higher than WT). For variant E138Q, the  $k_{cat}$  value was 1662.8  $\text{min}^{-1}$  (7.96-fold that of WT), with a  $K_m$  value 1.70 times higher than WT (8.9 mM), thus only resulting in a 1.67-fold increase in catalytic efficiency.

Furthermore, these seven variants were each coupled with *AaHycA* and *AtHycH* in cascade reactions with 100 mM 1a substrate. These results showed that A200E exhibited the highest catalytic efficacy, with a D-Trp yield of 97.8% at 24 h (Table 1), similar to that of variant R211G obtained by random mutagenesis. Variants A200S and E138W achieved respective product yields of 94.2% and 93.8% at 24 h. For A200N and S207A, slightly lower product yields of 92.7% and 92.4% were reached. Notably, variants with significantly reduced  $K_m$  values compared with WT gave high product yields, suggesting that high substrate affinity of NiHyc is critical for the cascade reaction, especially when substrate concentration is low in the late stage of the reaction.

*N*-Carbamoyl-tryptophan (3a), the substrate of NiHyc, is the product of the first two steps in the cascade process. 3a is accumulated at a relatively lower level during the reaction (Figure S11B–H). For WT (Figure S11A), the conversion of 3a is inhibited by its higher  $K_m$  (8.9 mM), whereas for variants with lower  $K_m$  values (1.1–4.5 mM), 3a can be more efficiently converted into D-Trp, which also promotes the overall efficiency of the cascade reaction process. Unexpectedly, the product yield of variant A200H was low (85.6%), despite its reduced  $K_m$  of 3.2 mM. In this reaction, the concentration of 3a was stabilized at around 12 mM after 6 h (Figure S11F), potentially due to the product inhibitory effect on A200H in the later stages of the cascade reaction (data not shown). For

variant E138Q, which had a higher  $K_m$  value (2.70 times of WT), the product yield was even lower (74.2%). These results demonstrate that a low  $K_m$  value for NiHyc may play an important role in the cascade reaction.

**Combinatorial Mutagenesis to Improve Catalytic Efficiency.** To further boost the catalytic efficiency of the NiHyc, iterative combinatorial mutagenesis was conducted on seven single mutants.<sup>36,37</sup> Three high-performing double mutants, E138W/R211G (M2-2), S207A/R211G (M2-3), and A200N/R211G (M2-4) (Table 1) were identified; more results are shown in Figure S12 and Table S3. Among them, variant M2-3 showed a reduced  $K_m$  value of 0.7 mM (7.87% of WT) and 9.70-fold enhanced  $k_{cat}/K_m$ . Then the reaction performance of M2-2, M2-3, and M2-4 was evaluated in a cascade reaction at 200 mM **1a**, and the yields were 63.8%, 66.4%, and 65.0%, representing 1.58, 1.66, and 1.62 times of WT (40.1%), respectively. Then each of these three variants was combined with other sites (E138W, D187N, A200N, and S207A) to construct triple mutants (Table S3). Among them, D187N/A200N/R211G (M3-1), D187N/S207A/R211G (M3-2), A200N/S207A/R211G (M3-3), and E138W/S207A/R211G (M3-4) exhibited significantly enhanced catalytic efficiency, with  $k_{cat}/K_m$  values of 807.5, 638.1, 630.9, and 600.2  $\text{min}^{-1} \text{mM}^{-1}$ , representing 22.35–30.42 times higher efficiency than that of WT (Table 1). Next, variants M3-1, M3-2, and M3-3 with lower  $K_m$  values (0.6–0.8 mM) were combined with sites (E138W, D187N, A200N, and S207A) to construct quadruple mutants (Table S3). The best variant, D187N/A200N/S207A/R211G (M4), exhibited 43.2 times higher efficiency ( $1135.0 \text{ min}^{-1} \text{mM}^{-1}$ ) than that of WT (Table 1). Variant M4 showed a  $K_m$  value of 0.4 mM, only 4.49% of WT (8.9 mM). Furthermore, the initial reaction rates of each variant in the cascade reaction (within 5 min) were 1.4 (R211G), 2.2 (M2-3), 5.5 (M3-1), and 6.4 (M4)  $\mu\text{mol min}^{-1} \text{mL}^{-1}$ , representing 2.58, 4.64, 13.1, and 15.4-fold higher rates than that of WT ( $0.39 \mu\text{mol min}^{-1} \text{mL}^{-1}$ ), respectively, corresponding to their enhanced  $k_{cat}/K_m$  (Figure S13).

The reaction performance of M3-1, M4, and WT was also evaluated in AaHycA/AiHycH-coupled cascade reactions at 200 mM **1a**. For best variant M4, 91.9% conversion and 79.1% product yield were achieved at 24 h, while only 40.1% yield was attained by WT (Table 1). Previous reports have shown that activities of D-carbamoylases may be inhibited by  $\text{NH}_3$  and D-amino acid products.<sup>38–41</sup> Cascade reactions with WT and M4 were then tested using a reduced substrate loading of 160 mM **1a**. This reduction in substrate resulted in respective yields of 94.8% and 47.6% for M4 and WT at 12 h (Figure S14). For M4, the residual **3a** was determined to be 5.56 mM, significantly lower than that of WT (31.4 mM), in accordance with its decreased  $K_m$ . Additionally, the half-life of M4 was determined to be 96 h at 30 °C, higher than that of WT (72 h). This finding indicates that enhanced substrate affinity could contribute to the elevated reaction performance of M4.

**Crystal Structures of NiHyc Variants.** To elucidate the evolutionary changes that lead to enhanced catalytic efficiency, crystal structures of variants R211G, M3-1, and M4 were resolved using WT NiHyc (6LEI) as a model and refined, specifically as 6LED (2.37 Å), 6LCG (2.70 Å), and 6LE2 (2.14 Å), all three of which form dimers with the same space group of P6122 (Tables S4 and S5). All structures have clear electron density at the catalytic center. On the basis of structure alignments of WT and three variants, loop 200–207 (involving mutation sites 200, 207) in the variants showed a gradual,

outward offset in R211G, M3-1, and M4 (Figure 4A,B). The distance between the centroid of Asp201 in WT and M4 was 9.35 Å. As shown in Figure 4C, loop 200–207 is located at the entrance of the substrate tunnel. Mutations A200N and S207A are both located on loop 200–207, and R211G lies on the  $\alpha$  helix that links to loop 200–207. In contrast, D187N is located on a loop that far away from the catalytic center. Interaction analysis was performed to better understand the loop swing (Figure 4B). For WT, an attractive electrostatic interaction was identified between Arg211 and Asp201 (Figure 4D). In addition, Arg211 was found to form hydrogen bonds with Ser207 and Glu206. These interactions may lead to a relatively strong attraction between Arg211 and loop 200–207. For M4, Gly211 was only found to form a hydrogen bond with Ala207 (Figure 4E). Therefore, fewer interactions between Gly211 and loop 200–207 were observed in M4 compared with WT, potentially resulting in enhanced loop flexibility. Additionally, higher B factors of loop 200–207 in M4 was observed when compared with that of WT (Figure S15).

Since the B factors observed in crystal structures are also dependent on crystallographic conditions, 500 ns MD simulations based on crystal structure were performed for both WT and M4 in order to validate the dynamic effects and to interrogate the structural rationalization (Figure S16). In WT, no hydrogen bond can be formed for the side chain of Ala200. However, in M4, the side chain of Asn200 forms two hydrogen bonds with water molecules (TIP6160 and TIP7483, Figure S17B). When exposed to solvent, the hydrogen bonds formed between Asn200 and water molecules will also increase the flexibility of loop 200–207.<sup>42</sup> Then, RMSF values of residues were determined for both WT and M4 using trajectory analysis (Figure S18), which revealed that the RMSF values of loop 200–207 of M4 were higher than that of WT. This result was consistent with the higher flexibility of loop 200–207 observed in the crystal structure of M4. Therefore, the enhanced flexibility of loop 200–207 in M4 may contribute to an outward loop swing (Figure 4B), which favors an open substrate tunnel, and is conducive to substrate access.

**MD Simulations of Prereaction States.** The prereaction states (PRS) of M4-3a and WT-3a were analyzed to facilitate clarification of the reaction mechanism. The prereaction state is defined as the conformation of the reacting enzyme–substrate complex prior to the critical transition state along the reaction coordinate, which is extracted from all of the possible substrate–enzyme complexations observed in the MD simulation.<sup>43–46</sup> Therefore, the relative stability of the PRS can reflect an enzyme–substrate fitness. According to the catalytic mechanism (Figure S19A) of D-carbamoylase,<sup>47</sup> Cys171 (-SH) acts as a nucleophile that initiates the reaction by attacking the C16 of **3a** (Figure 19B). Lys126 stabilizes the transient tetrahedral intermediate by carrying the O18 of **3a**, while Glu47 is responsible for proton transfer. In a typical nucleophilic attack reaction, the angle of nucleophilic attack (Bürgi–Dunitz angle, Figure S19C) describes the reacting conformation during the nucleophile approach to an electrophile,<sup>48,49</sup> which usually falls within the range of 100–110°. Thus, this angle is generally used to classify the reactive conformation.<sup>50–52</sup> According to data found in the Cambridge structural database summarized by Henry Rzepa,<sup>53</sup> the distance from the nucleophilic atom ( $S_{\text{Cys171}}$ ) to the carbon of carbonyl group could be as close as 3.5 Å. Therefore, the reactive conformation that satisfies both a nucleophilic attack

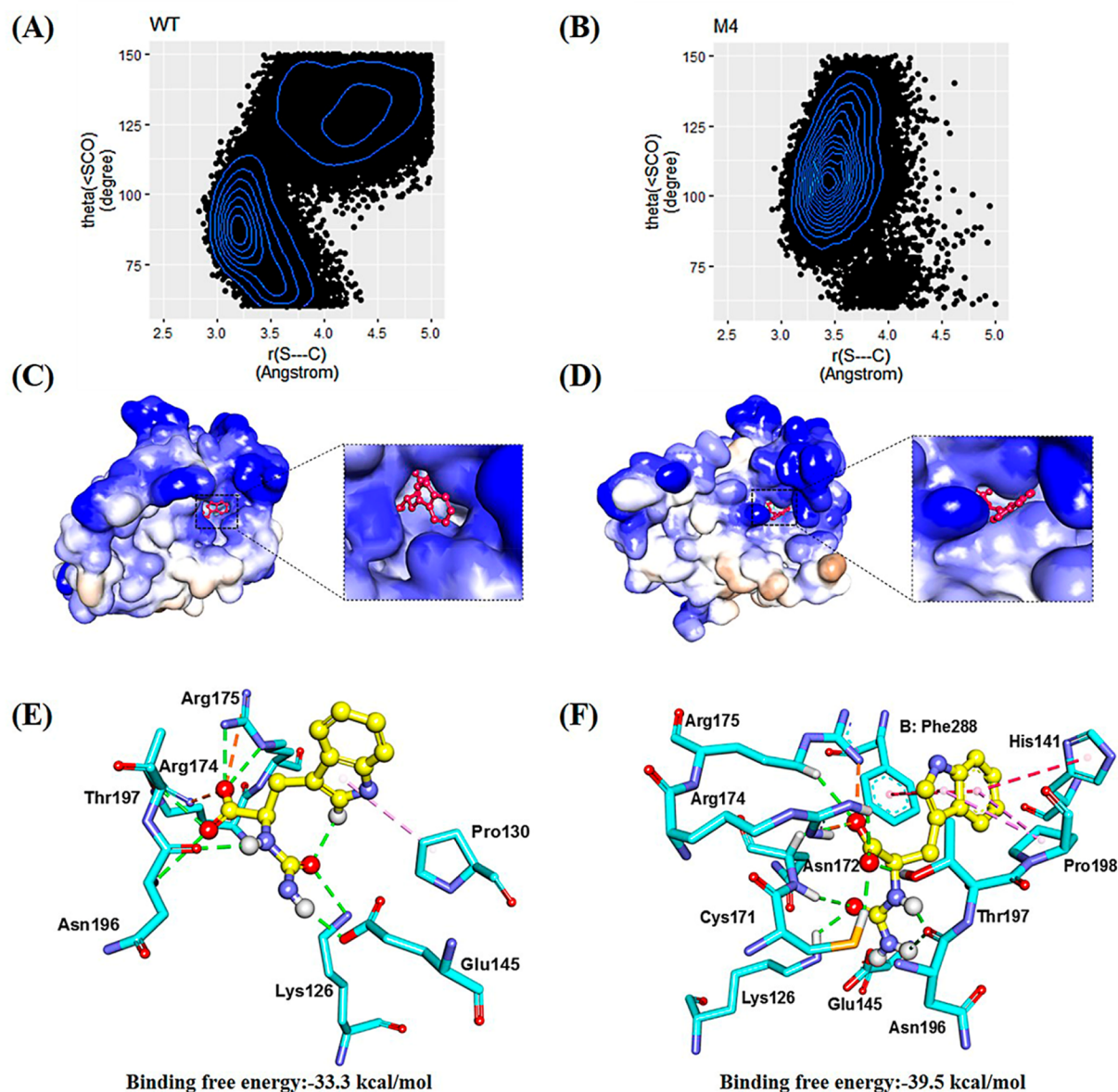


**Figure 5.** Analysis of prereaction states. Conformational distribution of (A) NiHyuC WT-3a and (B) variant M4-3a;  $r_{(S-C)}$ : the distance of  $S_{Cys171}$  to  $C16_{3a}$ ;  $\theta(\angle SCO)$ : nucleophilic attack angle. The prereaction states were performed using the complexes of WT-3a and M4-3a. The conformation satisfying both  $100^\circ \leq \theta \leq 110^\circ$  and  $r_{(S-C)} \leq 3.5$  Å is used for calculating the population of prereaction states. Substrate binding pocket of (C) NiHyuC WT-3a and (D) variant M4-3a in prereaction states. WT and M4 are shown in surface models. Substrate 3a is shown in magenta sticks. Interaction analysis of (E) WT-3a and (F) M4-3a. 3a is shown in yellow ball and sticks, residues in cyan sticks. Green dotted line indicates hydrogen bonds; magenta lines indicate  $\pi$ - $\pi$  stacking interactions; pink line indicates  $\pi$ -alkyl interactions; and orange line indicates salt bridges.

angle ( $S_{Cys171}$  attack to  $C16_{3a}$ ) of  $100^\circ \leq \theta \leq 110^\circ$  and an attack distance  $d$  ( $S_{Cys171}$ - $C16_{3a}$ ) of  $\leq 3.5$  Å is used for calculating the population of potential prereaction states (Figure S19D).

In order to explore the relative PRS population,  $6 \times 10$  ns MD simulations were performed for M4-3a and WT-3a substrate-enzyme complexes (Figure S20). These analyses revealed that the nucleophilic attack angle for WT was mostly distributed over the range of  $60^\circ$ - $100^\circ$  and  $120^\circ$ - $150^\circ$ , less than ideal, and only 6.4% of conformations fell into the range of  $100^\circ$ - $110^\circ$  (Figure 5A). However, in M4, the nucleophilic attack angle precisely aligned within the  $100^\circ$ - $110^\circ$  optimal range, and the proportion of conformations that matched the Bürgi-Dunitz angle were 26.4%, or 4.13 times that of WT

(Figure 5B). These results confirm that M4 has a more effective angle of nucleophilic attack, corresponding to the orientation of the carbonyl  $\pi^*$ -orbital. The Bürgi-Dunitz angle is well-known to be the product of overlap between lowest unoccupied molecular orbital (LUMO) of the carbonyl and the highest occupied molecular orbital (HOMO) of the nucleophile,<sup>48</sup> strongly suggesting that the elevated catalytic efficiency of M4 may be attributed to the increased interaction between LUMO and HOMO. The proportion of complexes in PRS is regarded as the degree of reaction readiness,<sup>54</sup> which was 14.6% for M4-3a, or 3.17 times that of WT-3a (4.6%), therefore suggesting that M4 has increased reaction readiness compared with WT.

In order to determine the underlying basis for the specific stability in the PRS in M4, the structural characteristics of M4–3a interactions in the PRS were closely analyzed. As shown in Figure 5C, substrate 3a binds in parallel to the spacious pocket of WT, whereas the reshaped M4 binding pocket is small and narrow, resulting in 3a binding perpendicular to the pocket (Figure 5D). This rotated 3a binding conformation leads to a greater number of interactions with M4. Compared with WT (Figure 5E), additional hydrogen bonds are formed between the carbamoyl group of 3a with Asn172 and Asn196 in M4 (Figure 5F). On the carboxyl side of 3a, two extra hydrogen bonds are formed with Cys171 and Arg174. Furthermore, the indole ring of 3a forms  $\pi$ – $\pi$  stacking interactions with His141 and B: Phe288, as well as a  $\pi$ -alkyl hydrophobic interaction with Pro198. Additionally, the binding free energies of WT–3a and M4–3a were calculated to be  $-33.3 \pm 3.1$  kcal mol<sup>-1</sup> and  $-39.5 \pm 3.9$  kcal mol<sup>-1</sup>, respectively, using the MM/GBSA method.<sup>55</sup> This is qualitatively consistent with the decreased  $K_m$  value of M4. Energy decomposition analysis reveals that there are changes in free energy during substrate binding at residues Asn187 ( $\Delta_{(M4-WT)}$ :  $-0.25$  kcal mol<sup>-1</sup>), Asn200 ( $\Delta_{(M4-WT)}$ :  $-0.22$  kcal mol<sup>-1</sup>), His141 ( $\Delta_{(M4-WT)}$ :  $-0.37$  kcal mol<sup>-1</sup>), Pro198 ( $\Delta_{(M4-WT)}$ :  $-0.38$  kcal mol<sup>-1</sup>), and B: Phe288 ( $\Delta_{(M4-WT)}$ :  $-0.59$  kcal mol<sup>-1</sup>), indicating that they play an essential role in substrate binding (Table S6). Although all four mutation sites in M4 (D187N, A200N, S207A, and R211G) have no direct interaction with 3a, their synergistic effect reshapes the substrate binding pocket, thereby promoting interactions between 3a and adjacent residues. Taken together, these results indicate that mutations restructure the binding pocket of M4 and resulted in a greater number of binding and stabilizing interactions with 3a in prereaction states, thereby conferring a higher affinity and catalytic efficiency for M4 toward 3a compared with WT.

**Substrate Spectrum of Variant M4.** The substrate spectrum and enantioselectivity of M4 were also determined (Figure 1). M4 displayed a high substrate specificity toward 3a and 3e. Compared with WT, M4 lost activity toward 3b and 3c. This is in accordance with the protein evolutionary theory; an evolved catalyst with enhanced catalytic efficiency in a specific reaction tends to lose its promiscuous activity.<sup>27</sup> Mutations may facilitate the reshaping of the substrate binding pocket of M4, which lost activity toward 3b and 3c. Interaction analysis of WT and M4 toward 3b and 3c revealed that in WT, for 3b, hydrogen bonds are formed with Glu145, Cys171, Arg174, Asn196, and Thr197. In addition, on the benzene ring side of 3b, a  $\pi$ -alkyl interaction with Pro130 and van der Waals forces with Gly131, His141, Pro198, and B: Ile285 were also observed (Figure S21A). In contrast, fewer hydrogen bonds were formed between 3b and M4, in addition to weak van der Waals force on the benzene ring side (Figure S21B). For 3c, major differences were identified between WT and M4 interactions with a side carrying the benzene ring moiety. In WT (Figure S21C), the benzene ring of 3c forms  $\pi$ -alkyl interaction with Pro130 and van der Waals forces with Pro198 and B: Ile285. Whereas, only weak van der Waals forces were observed between the benzene ring and B: Phe288 in M4 (Figure S21D). These results thus indicated that M4 exhibits lower affinity toward 3b and 3c, thereby preventing catalysis of these two substrates.

**Preparation of D-Trp in Cascade Reactions.** The performance of variant M4 in the preparation of D-Trp was

evaluated in a 0.5 L scale cascade reaction with 160 mM 1a. Complete conversion was achieved at 12 h, resulting in 159 mM D-Trp with 99.3% yield and productivity of 64.9 g L<sup>-1</sup> d<sup>-1</sup> (Figure S22). Compared with 20 mL reaction (94.8% yield), the higher yield could be attributed to the improved mass transfer in a 0.5 L scale. This result represents 4.41-fold higher productivity than that reported by Nozaki et al. (12.0 g L<sup>-1</sup> d<sup>-1</sup> at 48 h)<sup>21</sup> and 1.77-fold of previously reported cascade reactions using AcHyuC.<sup>34</sup> After purification, 12.7 g of D-Trp was obtained with an isolation yield of 78.0% and over 99.9% e.e. The product was confirmed to be D-Trp by chiral-HPLC and <sup>1</sup>H NMR analysis (Figure S23, S24).

## CONCLUSION

Here, a D-carbamoylase NiHyuC from *Nitratireductor indicus* CGMCC 1.10953 was obtained by gene database mining. Its high  $K_m$  value (8.9 mM) led to a relatively low  $k_{cat}/K_m$  of 25.7 min<sup>-1</sup> mM<sup>-1</sup>. Structure-guided engineering was used to increase the catalytic efficiency of NiHyuC, resulting in variant M4 (D187N/A200N/S207A/R211G), which exhibited 43-fold higher catalytic efficiency and 21-fold lower  $K_m$  value than WT. On the basis of crystal structures and MD simulations of WT and its variants, loop 200–207 may play an important role in modulating the substrate entrance tunnel. In M4, the enhanced flexibility of loop 200–207 facilitates an open entrance tunnel for substrate access. In MD simulations of prereaction states, M4 had a more effective nucleophilic attack angle and more readily formed prereaction states than WT. Additionally, M4 exhibited lower binding free energy than WT, qualitatively corresponding to its decreased  $K_m$  value. When applied in a cascade reaction, full conversion of 160 mM L-indolylmethylhydantoin was achieved by M4 in a 0.5 L reaction scale, with a D-Trp yield of 99.3% and productivity of 64.9 g L<sup>-1</sup> d<sup>-1</sup>. This study provides guidance for improvement of D-carbamoylase catalytic efficiency and reveals a key loop at the substrate entrance tunnel.

## ASSOCIATED CONTENT

### Supporting Information

The Supporting Information is available free of charge at <https://pubs.acs.org/doi/10.1021/acscatal.0c02942>.

Materials, cloning, protein expression and purification, enzyme activity assay and characterization, kinetic parameters, high-throughput screening method, random and saturation mutagenesis, crystallization and X-ray structural analysis, molecular docking and molecular dynamic simulations, analysis of prereaction state, preparation of optically D-Trp by cascade reaction and <sup>1</sup>H NMR analysis (PDF)

## AUTHOR INFORMATION

### Corresponding Authors

Ye Ni – Key Laboratory of Industrial Biotechnology, Ministry of Education, School of Biotechnology, Jiangnan University, Wuxi 214122, Jiangsu, China; [orcid.org/0000-0003-4887-7517](https://orcid.org/0000-0003-4887-7517); Email: [yeni@jiangnan.edu.cn](mailto:yeni@jiangnan.edu.cn)

Yi-Lei Zhao – State Key Laboratory of Microbial Metabolism, School of Life Sciences and Biotechnology, Shanghai Jiao Tong University, Shanghai 200240, China; [orcid.org/0000-0003-4687-7847](https://orcid.org/0000-0003-4687-7847); Email: [yileizhao@sjtu.edu.cn](mailto:yileizhao@sjtu.edu.cn)

Yijian Rao – Key Laboratory of Carbohydrate Chemistry and Biotechnology, Ministry of Education, School of Biotechnology,

Jiangnan University, Wuxi 214122, Jiangsu, China;  
orcid.org/0000-0003-2481-0588; Email: raoyijian@jiangnan.edu.cn

## Authors

**Yafei Liu** – Key Laboratory of Industrial Biotechnology, Ministry of Education, School of Biotechnology, Jiangnan University, Wuxi 214122, Jiangsu, China

**Guochao Xu** – Key Laboratory of Industrial Biotechnology, Ministry of Education, School of Biotechnology, Jiangnan University, Wuxi 214122, Jiangsu, China

**Jieyu Zhou** – Key Laboratory of Industrial Biotechnology, Ministry of Education, School of Biotechnology, Jiangnan University, Wuxi 214122, Jiangsu, China

**Jie Ni** – Warshel Institute for Computational Biology, School of Life and Health Science, Chinese University of Hong Kong (Shenzhen), Shenzhen 518172, China

**Lu Zhang** – Key Laboratory of Industrial Biotechnology, Ministry of Education, School of Biotechnology, Jiangnan University, Wuxi 214122, Jiangsu, China

**Xiaodong Hou** – Key Laboratory of Carbohydrate Chemistry and Biotechnology, Ministry of Education, School of Biotechnology, Jiangnan University, Wuxi 214122, Jiangsu, China

**Dejing Yin** – Key Laboratory of Industrial Biotechnology, Ministry of Education, School of Biotechnology, Jiangnan University, Wuxi 214122, Jiangsu, China

Complete contact information is available at:  
<https://pubs.acs.org/10.1021/acscatal.0c02942>

## Author Contributions

Y.L. and G.X. contributed equally to this work.

## Notes

The authors declare no competing financial interest.

## ACKNOWLEDGMENTS

We are grateful to the National Key Research and Development Program (2018YFA0901700, 2018YFA0901200), National Natural Science Foundation of China (22077054, 31970041, 21776112), and National First-Class Discipline Program of Light Industry Technology and Engineering (LITE2018-07). We thank the staffs from BL17B1 and BL18U1 at Shanghai Synchrotron Radiation Facility for assistance during data collection.

## REFERENCES

- (1) Gao, X. Z.; Ma, Q. Y.; Zhu, H. L. Distribution, Industrial Applications, and Enzymatic Synthesis of D-Amino Acids. *Appl. Microbiol. Biotechnol.* **2015**, *99*, 3341–3349.
- (2) Friedman, M.; Levin, C. E. Nutritional and Medicinal Aspects of D-Amino Acids. *Amino Acids* **2012**, *42*, 1553–1582.
- (3) Martínez-Rodríguez, S.; Martínez-Gómez, A. I.; Rodríguez-Vico, F.; Clemente-Jiménez, J. M.; Las Heras-Vázquez, F. J. Natural Occurrence and Industrial Applications of D-amino Acids: an Overview. *Chem. Biodiversity* **2010**, *7*, 1531–1548.
- (4) Global Industry Analysts, Inc. <https://www.strategyr.com/market-report-d-amino-acids-forecasts-global-industry-analysts-inc.asp> (accessed 2-2-2020).
- (5) Sugie, M.; Suzuki, H. Optical Resolution of DL-Amino Acids with D-Aminoacylase of *Streptomyces*. *Agric. Biol. Chem.* **1980**, *44*, 1089–1095.
- (6) Parmeggiani, F.; Lovelock, S. L.; Weise, N. J.; Ahmed, S. T.; Turner, N. J. Synthesis of D- and L-Phenylalanine Derivatives by

Phenylalanine Ammonia Lyases: a Multienzymatic Cascade Process. *Angew. Chem., Int. Ed.* **2015**, *54*, 4608–4611.

- (7) Nagy, E. Z. A.; Tork, S. D.; Lang, P. A.; Filip, A.; Irimie, F. D.; Poppe, L.; Tosa, M. I.; Schofield, C. J.; Brem, J.; Paizs, C.; Bencze, L. C. Mapping the Hydrophobic Substrate Binding Site of Phenylalanine Ammonia-Lyase from *Petroselinum crispum*. *ACS Catal.* **2019**, *9*, 8825–8834.

- (8) Han, S. W.; Shin, J. S. One-Pot Preparation of D-Amino Acids Through Biocatalytic Deracemization Using Alanine Dehydrogenase and  $\omega$ -Transaminase. *Catal. Lett.* **2018**, *148*, 3678–3684.

- (9) Yamamoto, H.; Mitsunashi, K.; Matsuyama, A.; Tomita, F. Method for Producing D-Tryptophan. U.S. US916781, 1999.

- (10) Greenstein, J. P. Resolution of DL Mixtures of  $\alpha$ -Amino Acids. *Methods Enzymol.* **1957**, *3*, 554–570.

- (11) Sylđatk, C.; Lufer, A.; Muller, R.; Hoke, H. Production of Optically Pure D- and L- $\alpha$ -Amino Acids by Bioconversion of D, L-5-Monosubstituted Hydantoin Derivatives. *Microb. Bioprod.* **1990**, *41*, 29–75.

- (12) Heras-Vazquez, F.; Clemente-Jimenez, J.; Martinez-Rodriguez, S.; Rodriguez-Vico, F. Optically Pure  $\alpha$ -Amino Acids Production by the “Hydantoinase Process. *Recent Pat. Biotechnol.* **2008**, *2*, 35–46.

- (13) Altenbuchner, J.; Siemann-Herzberg, M.; Sylđatk, C. Hydantoinases and Related Enzymes as Biocatalysts for the Synthesis of Unnatural Chiral Amino Acids. *Curr. Opin. Biotechnol.* **2001**, *12*, 559–563.

- (14) May, O.; Verseck, S.; Bommarius, A.; Drauz, K. Development of Dynamic Kinetic Resolution Processes for Biocatalytic Production of Natural and Non-natural L-Amino Acids. *Org. Process Res. Dev.* **2002**, *6*, 452–457.

- (15) Rodríguez-Alonso, M. J.; Clemente-Jiménez, J. M.; Rodríguez-Vico, F.; Las Heras-Vázquez, F. J. Rational Re-design of the “Double-Racemase Hydantoinase Process” for Optically Pure Production of Natural and Non-natural L-Amino Acids. *Biochem. Eng. J.* **2015**, *101*, 68–76.

- (16) Aranz, I.; Acosta, N.; Heras, A. Encapsulation of an *Agrobacterium radiobacter* Extract Containing D-Hydantoinase and D-Carbamoylase Activities into Alginate-Chitosan Polyelectrolyte Complexes: Preparation of the Biocatalyst. *J. Mol. Catal. B: Enzym.* **2009**, *58*, 54–64.

- (17) Kim, G. J.; Kim, H. S. Optimization of the Enzymatic Synthesis of D-p-Hydroxyphenylglycine from DL-5-Substituted Hydantoin Using D-Hydantoinase and N-carbamoylase. *Enzyme Microb. Technol.* **1995**, *17*, 63–67.

- (18) Martínez-Rodríguez, S.; Martínez-Gómez, A. I.; Rodríguez-Vico, F.; Clemente-Jiménez, J. M.; Las Heras-Vázquez, F. J. Carbamoylases: Characteristics and Applications in Biotechnological Processes. *Appl. Microbiol. Biotechnol.* **2010**, *85*, 441–458.

- (19) Ogawa, J.; Chung, M. C. M.; Hida, S.; Yamada, H.; Shimizu, S. Thermostable N-carbamoyl-D-amino Acid Amidohydrolase: Screening, Purification and Characterization. *J. Biotechnol.* **1994**, *38*, 11–19.

- (20) Oh, K. H.; Nam, S. H.; Kim, H. S. Improvement of Oxidative and Thermostability of N-carbamoyl-D-amino Acid Amidohydrolase by Directed Evolution. *Protein Eng., Des. Sel.* **2002**, *15*, 689–695.

- (21) Nozaki, H.; Takenaka, Y.; Kira, I.; Watanabe, K.; Yokozeki, K. D-Amino Acid Production by *E. coli* Co-expressed Three Genes Encoding Hydantoin Racemase, D-Hydantoinase and N-Carbamoyl-D-amino Acid Amidohydrolase. *J. Mol. Catal. B: Enzym.* **2005**, *32*, 213–218.

- (22) Martínez-Rodríguez, S.; Las Heras-Vázquez, F. J.; Clemente-Jimenez, J. M.; Mingorance-Cazorla, L.; Rodríguez-Vico, F. Complete Conversion of D, L-5-Monosubstituted Hydantoins with a Low Velocity of Chemical Racemization into D-Amino Acids Using Whole Cells of Recombinant *Escherichia coli*. *Biotechnol. Prog.* **2002**, *18*, 1201–1206.

- (23) Xu, G. C.; Wang, Y.; Tang, M. H.; Zhou, J. Y.; Zhao, J.; Han, R. Z.; Ni, Y. Hydroclassified Combinatorial Saturation Mutagenesis: Reshaping Substrate Binding Pockets of KpADH for Enantioselective Reduction of Bulky-Bulky Ketones. *ACS Catal.* **2018**, *8*, 8336–8345.

- (24) Zhou, J. Y.; Wang, Y.; Xu, G. C.; Wu, L.; Han, R. Z.; Schwaneberg, U.; Rao, Y. J.; Zhao, Y. L.; Zhou, J. H.; Ni, Y. Structural Insight into Enantioselective Inversion of an Alcohol Dehydrogenase Reveals a "Polar Gate" in Stereorecognition of Diaryl ketones. *J. Am. Chem. Soc.* **2018**, *140*, 12645–12654.
- (25) You, Z. N.; Chen, Q.; Shi, S. C.; Zheng, M. M.; Pan, J.; Qian, X. L.; Li, C. X.; Xu, J. H. Switching Cofactor Dependence of  $7\beta$ -Hydroxysteroid Dehydrogenase for Cost-Effective Production of Ursodeoxycholic Acid. *ACS Catal.* **2019**, *9*, 466–473.
- (26) Chen, F. F.; Zheng, G. W.; Liu, L.; Li, H.; Chen, Q.; Li, F. L.; Li, C. X.; Xu, J. H. Reshaping the Active Pocket of Amine Dehydrogenases for Asymmetric Synthesis of Bulky Aliphatic Amines. *ACS Catal.* **2018**, *8*, 2622–2628.
- (27) Pavlidis, I. V.; Weiß, M. S.; Genz, M.; Spurr, P.; Hanlon, S. P.; Wirz, B.; Iding, H.; Bornscheuer, U. T. Identification of (S)-Selective Transaminases for the Asymmetric Synthesis of Bulky Chiral Amines. *Nat. Chem.* **2016**, *8*, 1076–1082.
- (28) Li, A. T.; Ilie, A.; Sun, Z. T.; Lonsdale, R.; Xu, J. H.; Reetz, M. T. Whole-Cell-Catalyzed Multiple Regio- and Stereoselective Functionalizations in Cascade Reactions Enabled by Directed Evolution. *Angew. Chem., Int. Ed.* **2016**, *55*, 12026–12029.
- (29) Zhou, H. Y.; Wang, B. J.; Wang, F.; Yu, X. J.; Ma, L. X.; Li, A. T.; Reetz, M. T. Chemo- and Regioselective Dihydroxylation of Benzene to Hydroquinone Enabled by Engineered Cytochrome P450 Monooxygenase. *Angew. Chem., Int. Ed.* **2019**, *58*, 764–768.
- (30) Xia, B.; Xu, J.; Xiang, Z. W.; Cen, Y. X.; Hu, Y. J.; Lin, X. F.; Wu, Q. Stereoselectivity-Tailored, Metal-Free Hydrolytic Dynamic Kinetic Resolution of Morita–Baylis–Hillman Acetates Using an Engineered Lipase–Organic Base Cocatalyst. *ACS Catal.* **2017**, *7*, 4542–4549.
- (31) Xu, J.; Cen, Y.; Singh, W.; Fan, J.; Wu, L.; Lin, X.; Zhou, J.; Huang, M.; Reetz, M. T.; Wu, Q. Stereodivergent Protein Engineering of a Lipase to Access All Possible Stereoisomers of Chiral Esters with Two Stereocenters. *J. Am. Chem. Soc.* **2019**, *141*, 7934–7945.
- (32) Ikenaka, Y.; Nanba, H.; Yajima, K.; Yamada, Y.; Takano, M.; Takahashi, S. Increase in Thermostability of *N*-Carbamoyl-D-amino Acid Amidohydrolase on Amino Acid Substitutions. *Biosci., Biotechnol., Biochem.* **1998**, *62*, 1668–1671.
- (33) Chien, H.-C. R.; Hsu, C. L.; Hu, H. Y.; Wang, W. C.; Hsu, W. H. Enhancing Oxidative Resistance of *Agrobacterium radiobacter* *N*-Carbamoyl-D-amino Acid Amidohydrolase by Engineering Solvent-Accessible Methionine Residues. *Biochem. Biophys. Res. Commun.* **2002**, *297*, 282–287.
- (34) Liu, Y. F.; Xu, G. C.; Han, R. Z.; Dong, J. J.; Ni, Y. Identification of D-Carbamoylase for Biocatalytic Cascade Synthesis of D-Tryptophan Featuring High Enantioselectivity. *Bioresour. Technol.* **2018**, *249*, 720–728.
- (35) Nestl, B. M.; Hauer, B. Engineering of Flexible Loops in Enzymes. *ACS Catal.* **2014**, *4*, 3201–3211.
- (36) Sun, Z. T.; Lonsdale, R.; Kong, X. D.; Xu, J. H.; Zhou, J. H.; Reetz, M. T. Reshaping an Enzyme Binding Pocket for Enhanced and Inverted Stereoselectivity: Use of Smallest Amino Acid Alphabets in Directed Evolution. *Angew. Chem., Int. Ed.* **2015**, *54*, 12410–12415.
- (37) Reetz, M. T.; Bocola, M.; Carballeira, J. D.; Zha, D. X.; Vogel, A. Expanding the Range of Substrate Acceptance of Enzymes: Combinatorial Active-Site Saturation Test. *Angew. Chem., Int. Ed.* **2005**, *44*, 4192–4196.
- (38) Louwrier, A.; Knowles, C. J. The Purification and Characterization of a Novel D (–)-Specific Carbamoylase Enzyme from an *Agrobacterium* sp. *Enzyme Microb. Technol.* **1996**, *19*, S62–S71.
- (39) Nanba, H.; Ikenaka, Y.; Yamada, Y.; Yajima, K.; Takano, M.; Takahashi, S. Isolation of *Agrobacterium* sp. Strain KNK712 that Produces *N*-Carbamoyl-D-amino Acid Amidohydrolase, Cloning of the Gene for this Enzyme, and Properties of the Enzyme. *Biosci., Biotechnol., Biochem.* **1998**, *62*, 875–881.
- (40) Ogawa, J.; Shimizu, S.; Yamada, H. *N*-Carbamoyl-D-amino Acid Amidohydrolase from *Comamonas* sp. E222c Purification and Characterization. *Eur. J. Biochem.* **1993**, *212*, 685–691.
- (41) Olivieri, R.; Fascetti, E.; Angelini, L.; Degen, L. Enzymatic Conversion of *N*-carbamoyl-D-Amino Acids to D-Amino Acids. *Enzyme Microb. Technol.* **1979**, *1*, 201–204.
- (42) Tournier, A. L.; Xu, J. C.; Smith, J. C. Solvent Caging of Internal Motions in Myoglobin at Low Temperatures. *PhysChemComm* **2003**, *6*, 6–8.
- (43) He, B. B.; Zhou, T.; Bu, X. L.; Weng, J. Y.; Xu, J.; Lin, S. J.; Zheng, J. T.; Zhao, Y.-L.; Xu, M. J. Enzymatic Pyran Formation Involved in Xiamenmycin Biosynthesis. *ACS Catal.* **2019**, *9*, 5391–5399.
- (44) Zhang, Z.; Jamieson, C. S.; Zhao, Y.-L.; Li, D.; Ohashi, M.; Houk, K. N.; Tang, Y. Enzyme-Catalyzed Inverse-Electron Demand Diels-Alder Reaction in the Biosynthesis of Antifungal Ilicicolin H. *J. Am. Chem. Soc.* **2019**, *141*, 5659–5663.
- (45) Shi, T.; Liu, L.; Tao, W.; Luo, S.; Fan, S.; Wang, X. L.; Bai, L.; Zhao, Y.-L. Theoretical Studies on the Catalytic Mechanism and Substrate Diversity for Macrocyclization of Pikromycin Thioesterase. *ACS Catal.* **2018**, *8*, 4323–4332.
- (46) Chen, X.-P.; Shi, T.; Wang, X.-L.; Wang, J.; Chen, Q.; Bai, L.; Zhao, Y.-L. Theoretical Studies on the Mechanism of Thioesterase-Catalyzed Macrocyclization in Erythromycin Biosynthesis. *ACS Catal.* **2016**, *6*, 4369–4378.
- (47) Nakai, T.; Hasegawa, T.; Yamashita, E.; Yamamoto, M.; Kumasaka, T.; Ueki, T.; Nanba, H.; Ikenaka, Y.; Takahashi, S.; Sato, M.; Tsukihara, T. Crystal Structure of *N*-carbamoyl-D-amino Acid Amidohydrolase with a Novel Catalytic Framework Common to Amidohydrolases. *Structure* **2000**, *8*, 729–737.
- (48) Burgi, H.B.; Dunitz, J.D.; Lehn, J.M.; Wipff, G. Stereochemistry of Reaction Paths at Carbonyl Centres. *Tetrahedron* **1974**, *30*, 1563–1572.
- (49) Bürgi, H. B.; Dunitz, J. D.; Shefter, E. Chemical Reaction Paths. IV. Aspects of O···C=O Interactions in Crystals. *Acta Crystallogr., Sect. B: Struct. Crystallogr. Cryst. Chem.* **1974**, *30*, 1517–1527.
- (50) Sadiq, S. K.; Coveney, P. V. Computing the Role of Near Attack Conformations in an Enzyme-Catalyzed Nucleophilic Bimolecular Reaction. *J. Chem. Theory Comput.* **2015**, *11*, 316–324.
- (51) Syrén, P. O.; Hult, K. Substrate Conformations Set the Rate of Enzymatic Acylation by Lipases. *ChemBioChem* **2010**, *11*, 802–810.
- (52) Lightstone, F. C.; Bruice, T. C. Ground State Conformations and Entropic and Enthalpic Factors in the Efficiency of Intramolecular and Enzymatic Reactions. 1. Cyclic Anhydride Formation by Substituted Glutarates, Succinate, and 3, 6-Endoxo- $\Delta^4$ -tetrahydrophthalate Monophenyl esters. *J. Am. Chem. Soc.* **1996**, *118*, 2595–2605.
- (53) Rzepa, H. The Bürgi–Dunitz Angle Revisited: a Mystery? *Winnower* **2015**, *2*, No. e143149.99424.
- (54) Fan, S.; Wang, R.; Li, C.; Bai, L.; Zhao, Y.-L.; Shi, T. Insight into Structural Characteristics of Protein-Substrate Interaction in Pimaricin Thioesterase. *Int. J. Mol. Sci.* **2019**, *20*, 877.
- (55) Sun, H.; Li, Y.; Shen, M.; Tian, S.; Xu, L.; Pan, P.; Guan, Y.; Hou, T. Assessing the Performance of MM/PBSA and MM/GBSA Methods. 5. Improved Docking Performance Using High Solute Dielectric Constant MM/GBSA and MM/PBSA Rescoring. *Phys. Chem. Chem. Phys.* **2014**, *16*, 22035–22045.